

# New Photochrome Probe Allows Simultaneous pH and Microviscosity Sensing

Yuanyuan Wu<sup>1</sup> · Vladislav Papper<sup>1</sup> · Oleksandr Pokholenko<sup>1</sup> · Vladimir Kharlanov<sup>2</sup> · Yubin Zhou<sup>1</sup> · Terry W. J. Steele<sup>1</sup> · Robert S. Marks<sup>1</sup>

Received: 9 April 2015 / Accepted: 24 April 2015 / Published online: 19 May 2015  
© Springer Science+Business Media New York 2015

**Abstract** 4-*N,N'*-dimethylamino-4'-*N'*-stilbenemaleamic acid (DASMA), a unique molecular photochrome probe that exhibits solubility and retains *trans-cis* photoisomerisation in a wide range of organic solvents and aqueous pH environments, was prepared, purified and chemically characterised. Absorption, fluorescence excitation and emission spectra and constant-illumination fluorescence decay were measured in acetonitrile, dimethyl sulfoxide, ethanol, propylene carbonate, and aqueous glycerol mixtures. The pseudo-first-order fluorescence decay rates were found to be strongly dependent on the medium viscosity. In addition, the molecule exhibited the pH-dependent fluorescence and photoisomerisation kinetics.

**Keywords** Stilbene · Maleamic acid · Fluorescence · Photoisomerisation · Intramolecular charge transfer · pH sensor · Microviscosity · Viscosity sensor · Photochrome probe

## Abbreviations

DASMA	4- <i>N,N'</i> -dimethylamino-4'-stilbenemaleamic acid
ICT	Intramolecular charge transfer
DMA	Dimethylamino group
ACN	Acetonitrile
EtOH	Ethanol

**Electronic supplementary material** The online version of this article (doi:10.1007/s10895-015-1577-2) contains supplementary material, which is available to authorized users.

✉ Vladislav Papper  
vladp6@gmail.com

<sup>1</sup> School of Materials Science and Engineering, Nanyang Technological University, Singapore, Singapore

<sup>2</sup> Institute of Physical Chemistry, Humboldt University of Berlin, Berlin, Germany

DMSO	Dimethyl sulfoxide
PC	Propylene carbonate
DAAS	4-( <i>N,N'</i> -dimethylamino)-4'-aminostilbene

## Introduction

So far, stilbene compounds have never been widely used as molecular sensing entities in various biosensing devices and bioassays, although they possess all the desired features of the ideal reporter molecules, such as chemical and biological stability, relatively low toxicity, synthetic availability, high photochemical sensitivity, rapid response in solution without the need of a solid-phase assay, and easy regeneration. This is mainly because of their strong tendency to lose fluorescence rapidly upon excitation via the non-radiative deactivation process connected to the twisted transition in the excited state [1, 2]. The latter is responsible for the *trans-cis* photoisomerisation of the molecule and acts as a quenching funnel on fluorescence emission, thereby depriving the fluorescence probe of its photochemical stability.

As schematically shown on Fig. 1, many stilbene compounds can rapidly change their molecular configuration upon irradiation at the excitation maximum, if they are not sterically or electronically restricted to do so. The *trans-cis* photoisomerisation process is experimentally observed at the constant-illumination conditions as the rapid steady-state fluorescence decay to the photostationary equilibrium between the two isomers. Such photochemical instability could be a huge problem if the stilbene compound is considered a classical fluorescence probe, and this is probably the reason why stilbene compounds have never been effectively used in chemical, biological and biomedical applications.

However, the actual reporting power of the stilbenes is not in their fluorescence, but in a rapid loss of their fluorescence via an instant conformational change upon irradiation with the excitation light. This makes the stilbene switches unique in the sense that most fluorescent reporters (labels or probes) either

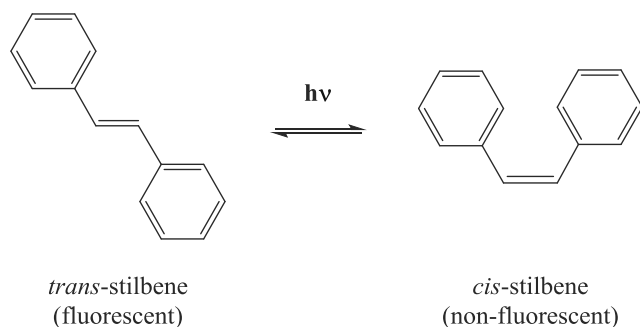


**Fig. 1** Stilbene exists in two molecular configurations: the fluorescent *trans*-isomer is switched to the non-fluorescent *cis*-isomer upon irradiation at the excitation maximum

do not possess this intramolecular switchable nature or require the separation of adjacent fluorophores.

In view of the above, one of the most striking features of stilbene photochemistry is its essentially strong dependence on medium properties, which can effectively alter or even hinder the photoisomerisation of the molecule in the excited state. We have previously shown a clear evidence that the *trans-cis* photoisomerisation of stilbene compounds is very sensitive to medium microviscosity and can be used in various applications [3–5].

Our new fluorescence-photochrome method was used for investigation of local medium effects and phase transitions in biological membranes and on solid surfaces [3–5]. The method is based on monitoring the *trans-cis* photoisomerisation

kinetics of stilbenes incorporated into an object of interest. It has been shown that the apparent rate constant of the *trans-cis* photoisomerisation in a relatively viscous media, for instance, in biological membranes, is controlled by the medium relaxation rate [4]. This method was also applied to studies of the microviscosity effects on the *trans-cis* photoisomerisation of the stilbene molecules immobilized onto quartz plates coated with lysozyme [5]. The apparent *trans-cis* photoisomerisation rate constant of the process was found to be 3–4 times lower for the immobilised stilbene molecule than for the same free molecule in solution. This indicated that the surface and the protein sterically hindered the twisting motion of the stilbene molecule in the excited state.

In addition, pH value can be also considered a critical parameter in many biological processes, for example, proper pH range ensures the success of many enzymatic reactions in intracellular compartments, such as the low pH environments within endosome and lysosome organelles. The abrupt change in pH within these environments is the basis for several ‘smart polymer’ drug delivery platforms [19]. Polyester synthetic materials are also known to harbour acidic pH microenvironments within neutral buffers, however the pH zones can only be measured indirectly with no simple techniques available to simultaneously measure the microenvironment material properties, i.e. microviscosity [20]. Therefore, a probe which simultaneously senses the microviscosity and pH, can be

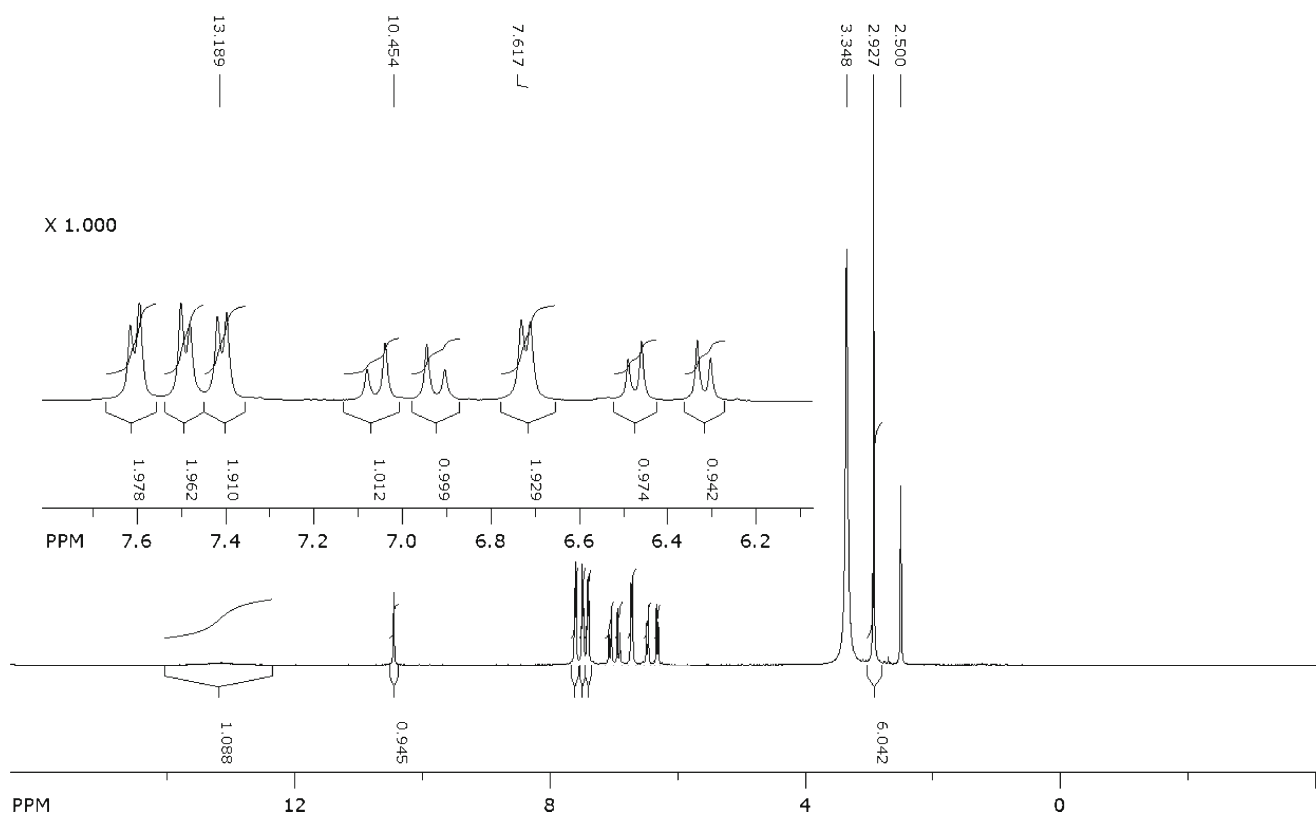


**Fig. 2**  $^1\text{H}$  NMR spectra of DASMA with extension in the aromatic region

invaluable in polymer research, and in other chemical and biological applications.

Herein, we report the synthetic preparation, and theoretical and experimental studies of 4-*N,N'*-dimethylamino-4'-*N*-stilbenemaleamic acid (DASMA), a unique molecular photochrome probe that exhibits solubility and retains conformational flexibility, i.e. *trans-cis* photoisomerisation in a wide range of organic solvents and aqueous pH environments. With a 'click chemistry' the functional group of the molecule can be incorporated for ease of chemical grafting, while the molecular sensing group can monitor changes in both pH- and microviscosity simultaneously.

## Experimental

### Reactants and Solvents

Reactants were either commercially available or freshly prepared as detailed in the [Synthesis](#) section. Organic solvents for spectroscopic measurements (spectroscopic grade) and for organic synthesis (ACS grade) were purchased from Sigma and

used without further purification. The buffer phosphate solution (5.65 mM NaH<sub>2</sub>PO<sub>4</sub>; 4.35 mM Na<sub>2</sub>HPO<sub>4</sub>; 10 mM MgCl<sub>2</sub>; 1 mM NaCl) used for pH-dependent spectroscopic studies was freshly prepared in our laboratory. Deionised (DI) water was supplied by Milli-Q® water system.

### Apparatus and Methods

Preparative flash chromatography used for purification of the compounds was performed with the Büchi Sepacore® flash chromatography system using 12 g reversed phase Sepacore® cartridges and 0.5 % aqueous NaHCO<sub>3</sub>/ethanol gradient.

<sup>1</sup>H and <sup>13</sup>C NMR spectra were run on 2 % (w/v) sample solutions in DMSO d<sub>6</sub> calibrating by the solvent residue peak being at 2.50 ppm at room temperature using a 400 MHz Bruker Fourier transform spectrometer, equipped with a DMX AVANCE I system. The collected NMR spectra were analysed using MestreNov. 9 (Mestrelab Research) and SpinWorks© 4.0.5 (Kirk Marat, University of Manitoba) software.

UV absorption spectra were measured using an Agilent Cary 300 spectrophotometer, and the fluorescence spectra

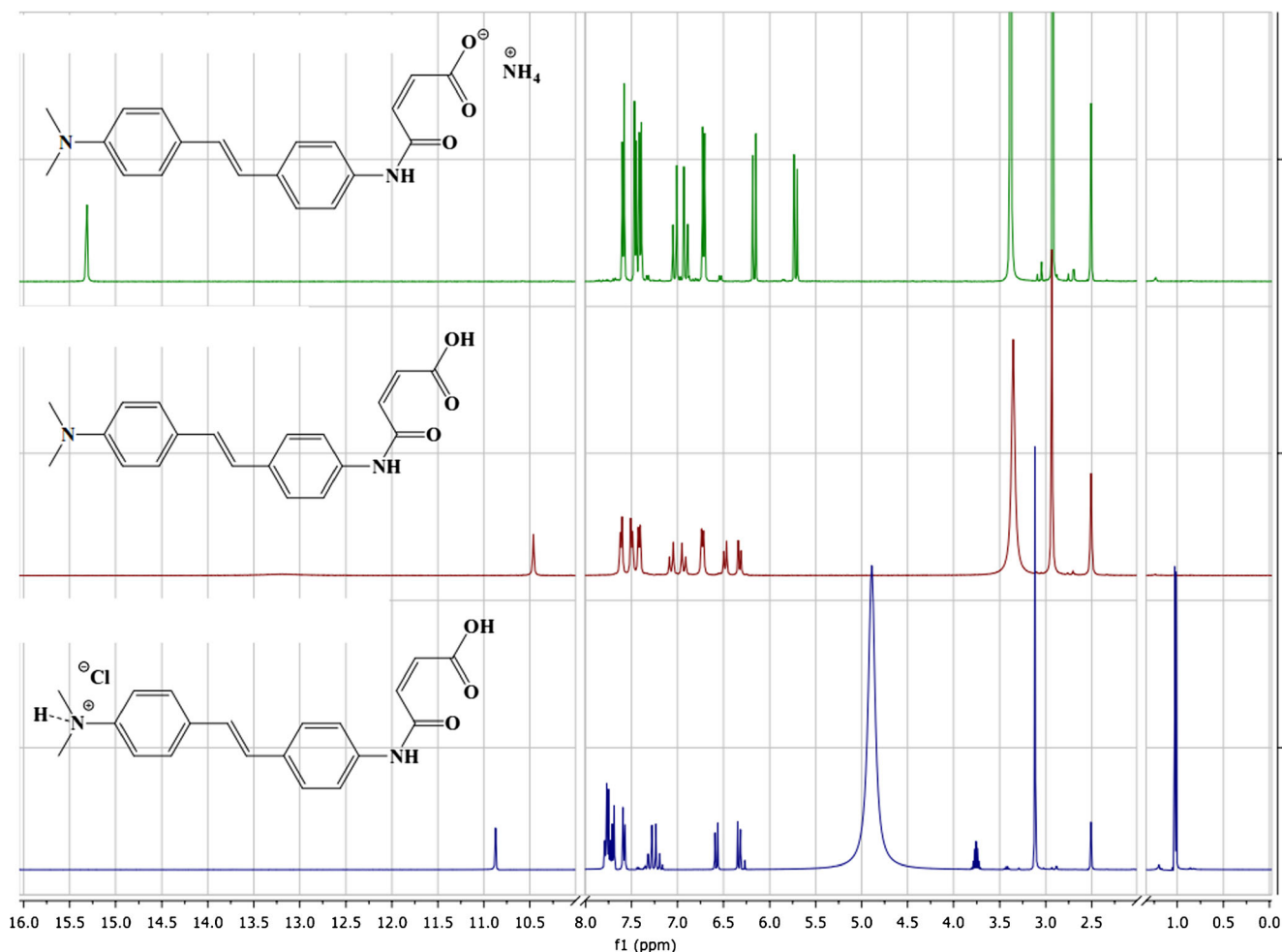


**Fig. 3** Comparative <sup>1</sup>H NMR spectra of DASMA and its salts

were recorded with Horiba Jobin Yvon FluoroLog®-3 modular spectrofluorometer.

Fluorescence excitation and emission spectra were corrected for instrumental sensitivity at different excitation and emission slits using the instrument internal excitation-emission matrix (EEM) correction [6]. A solution of quinine bisulphate in 0.1 N H<sub>2</sub>SO<sub>4</sub> ( $\Phi_f=0.52$ ) was taken as a fluorescence standard for the determination of fluorescence quantum yields [7].

Constant-illumination fluorescence decay curves at the photostationary steady-state equilibrium between the *trans* and *cis*-isomers of the investigated molecule were recorded with Shimadzu RF-5301 spectrofluorometer equipped with the 150 W Xenon lamp as a radiation light source. Fluorescence decay at the photostationary equilibrium was monitored at the emission maximum of the molecule after excitation at the excitation maximum using typically 5-nm slit width for excitation and 5-nm slit width for emission.

Viscosity of the DMSO and glycerol mixtures was measured using the Brookfield® viscometer.

Mass spectroscopy analysis was performed on a Shimadzu Biotech Axima TOF<sup>2</sup> in linear positive mode with factory calibration. Samples were spotted both *neat* and with DBA matrix.

Analysis of the experimental data was performed using Origin® Pro 9.0 for Windows. Fluorescence intensity decay

curves were analysed with an exponential fit for calculation of the *trans-cis* isomerisation apparent rate constants using a self-written routine within the Origin® Pro 9.0 for analysis of the pseudo-first-order photochemical reaction rates.

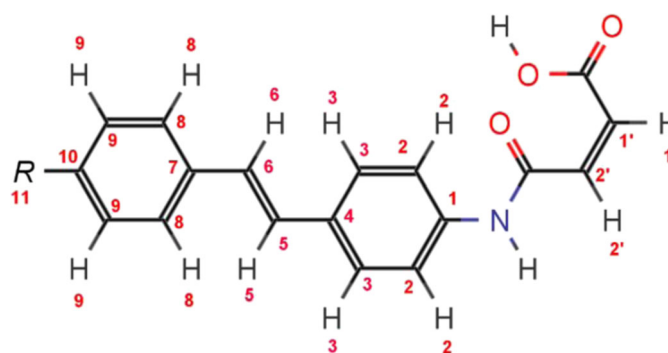
## Synthesis

The following reactants were prepared according to our procedure that we previously published in [8, 9]: *trans*-4-(*N,N'*-dimethylamino)-4'-nitrostilbene and *trans*-4-(*N,N'*-dimethylamino)-4'-aminostilbene.

### *trans*-4-*N,N'*-Dimethylamino-4'-*N*-Stilbenemaleamic Acid (DASMA)

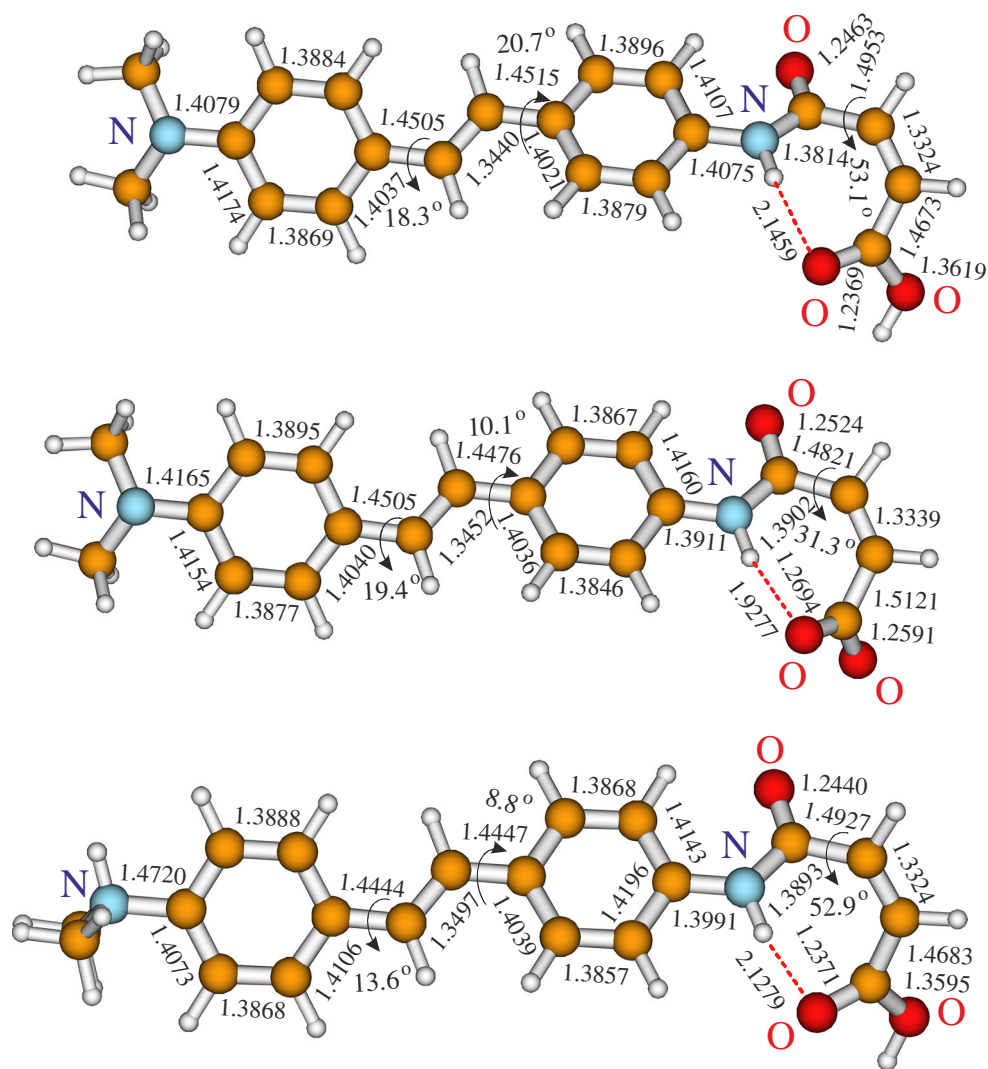
*trans*-4'-(*N,N'*-Dimethylamino)-4-aminostilbene (7.946 g, 33.34 mmol) was dissolved in 100 mL of dichloromethane. Maleic anhydride (Sigma-Aldrich 63200 Fluka) (4.34 g, 44.26 mmol) was dissolved in 50 mL of dichloromethane. The solutions were mixed and the mixture was left stirred for 4 h at room temperature. Black-coloured precipitate was formed and collected by vacuum filtration, washed with dichloromethane, dissolved in hot dimethyl formamide at 100 °C, and precipitated with water. Further purification was carried out by washing with water and diethyl ether to produce

**Table 1** Chemical shifts of DASMA, DASMA anion and DASMA cation in DMSO d<sub>6</sub>



	<sup>1</sup> H DASMA neutral	<sup>1</sup> H DASMA anion NH <sub>4</sub> <sup>+</sup> salt	<sup>1</sup> H DASMA cation Cl <sup>-</sup> salt
DMSO d <sub>6</sub> residual peak	2.500 ppm	2.500 ppm	2.500 ppm
Water in DMSO d <sub>6</sub>	3.348 ppm	3.376 ppm	4.883 ppm
H1'	6.333–6.302 ppm (1H d; 12.1 Hz)	5.728–5.694 ppm (1H d; 13.4 Hz)	6.337–6.307 ppm (1H d; 12.0 Hz)
H2'	6.489–6.459 ppm (1H d; 12.0 Hz)	6.174–6.141 ppm (1H d; 13.3 Hz)	6.585–6.554 ppm (1H d; 12.1 Hz)
H8	6.732–6.711 ppm (2H d; 8.3 Hz)	6.720–6.697 ppm (2H d; 8.9 Hz)	7.586–7.564 ppm (2H d; 8.7 Hz)
H6	6.946–6.905 ppm (1H d; 16.6 Hz)	6.924–6.882 ppm (1H d; 16.5 Hz)	7.228–7.187 ppm (1H d; 16.4 Hz)
H5	7.080–7.040 ppm (1H d; 16.3 Hz)	7.043–7.002 ppm (1H d; 16.2 Hz)	7.312–7.271 ppm (1H d; 16.5 Hz)
H9	7.420–7.399 ppm (2H d; 8.5 Hz)	7.408–7.386 ppm (2H d; 8.8 Hz)	7.704–7.682 ppm (2H d; 8.7 Hz)
H2	7.502–7.481 ppm (2H d; 8.3 Hz)	7.462–7.440 ppm (2H d; 8.7 Hz)	7.744–7.721 ppm (2H d; 9.0 Hz)
H3	7.617–7.596 ppm (2H d; 8.3 Hz)	7.595–7.573 ppm (2H d; 8.8 Hz)	7.785–7.763 ppm (2H d; 8.9 Hz)
CONH	10.454 ppm (1H s)	15.314–15.304 ppm (1H two broad s)	10.865 ppm (1H s)
COOH	13.185 ppm (1H broad s)	None	Under ~4.8 ppm (water peak)
R11	2.927 ppm (6H s; Me <sub>2</sub> N-)	2.918 ppm (6H s; Me <sub>2</sub> N-)	3.109 ppm (6H s; Me <sub>2</sub> N-)

**Fig. 4** Calculated geometry including bond lengths and torsion angles for DASMA neutral (*top*), DASMA anion (*middle*) and DASMA cation (*bottom*) calculated by semi-empirical methods



the final dark-red-coloured compound. Yield 85.7 % (9.61 g, 28.57 mmol).

$^1\text{H}$  NMR is shown in Figs. 2 and 3, summarised in Table 1, and will be discussed below.

$^{13}\text{C}$  NMR (100 MHz;  $\text{DMSO-}d_6$ ):  $\delta$  ppm 167.30; 163.49; 150.30; 137.55; 134.14; 131.97; 131.13; 128.28; 127.84; 126.72; 125.64; 123.62; 120.16; 112.80; 40.48.

MALDI TOF: exact mass ( $\text{C}_{20}\text{H}_{20}\text{N}_2\text{O}_3$ ) = 336.1474; found  $[\text{M}+\text{H}]^+ + 337$  Da.

### Ammonium

#### *trans*-4-*N,N'*-Dimethylamino-4'-*N*-Stilbenemaleamate (DASMA Anion)

DASMA (10 mg) was suspended in 0.5 mL  $\text{DMSO } d_6$  in an NMR tube, and transformed into the ammonium salt with 10  $\mu\text{L}$  of 30 % aqueous ammonia. After stirring, most of the solid was dissolved, and the originally formed red dispersion turned into transparent bright yellow solution. The prepared

sample was used for NMR studies. The obtained ammonium salt of DASMA was found to be very stable. It was stored in DMSO solution for 6 months without decomposition (see Fig. S8 in the Supplementary Information).

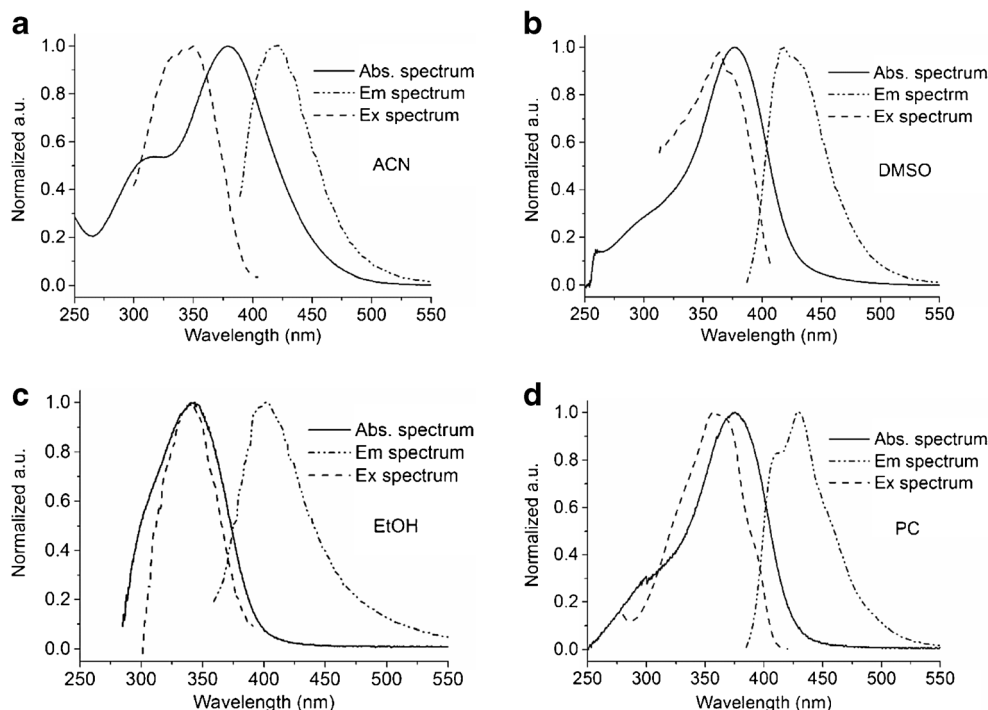
$^1\text{H}$  NMR is shown in Fig. 3, summarised in Table 1, and will be discussed below.

$^{13}\text{C}$  NMR (100 MHz;  $\text{DMSO-}d_6$ ):  $\delta$  ppm 169.06; 164.18; 150.24; 140.08; 139.11; 132.90; 130.51; 127.71; 127.48; 126.73; 125.77; 123.94; 119.55; 112.78; 40.47

**Table 2** Summary of the absolute energy (kcal/mol) of the AM1 optimised equilibrium structures, their transition energy  $\Delta E$  (oscillator strength  $f$ ), and dipole moment calculated by semi-empirical ZINDO/s

Compound	Energy, a.u.	$\Delta E$ , eV ( $f$ )	$\mu_{\text{g}}$ , D
DASMA	-0.0523714	3.50 (1.19); 357 nm	1.50
DASMA anion	-0.1057619	3.42 (1.32); 363 nm	–
DASMA cation	0.1841072	3.20 (1.18); 388 nm	–

**Fig. 5** Absorption, fluorescence excitation and emission spectra of DASMA in four solvents: AcCN (a), DMSO (b), EtOH (c) and PC (d)



### *trans*-4-*N,N'*-Dimethylamino-4'-*N*-Stilbenmaleamic Acid Hydrochloride (DASMA Cation)

DASMA (10 mg) was suspended in 0.6 mL DMSO and heated at 50 °C until complete dissolution. Addition of one drop (16 mg) of 37 % aq. HCl resulted in transparent green-yellow solution. This solution was transferred to a flask and kept under reduced pressure (30 mbar) at 50 °C for about 3 h. <sup>1</sup>H and <sup>13</sup>C NMR were recorded and the spectra revealed some traces of decomposition.

<sup>1</sup>H NMR is shown in Fig. 3, summarised in Table 1, and will be discussed below.

<sup>13</sup>C NMR (100 MHz; DMSO-*d*<sub>6</sub>): δ ppm 167.44; 163.66; 142.62; 138.86; 138.64; 132.77; 131.53; 131.45; 130.26; 128.03; 127.69; 126.18; 121.66; 120.15; 45.92.

### HPLC-DAD Analysis of the Synthesized DASMA

An Agilent 1200 Series LC system with diode array detector (DAD) and 5 μm, 4.6 mm×250 mm Ultisil™ C18 column (Welch Materials Inc.) was used to analyze the synthesised DASMA compound with a flow rate of 1 mL/min.

**Table 3** Absorption, fluorescence excitation and emission maximum wavelengths, molar extinction coefficient, fluorescence quantum yield, and apparent steady-state isomerisation rate constant for DASMA in different solvents

	λ (abs), nm	λ (ex), nm	λ (em), nm	ε, (M×cm) <sup>-1</sup>	Φ <sub>f</sub> , %	k <sub>app</sub> , s <sup>-1</sup>
AcCN	379	350	418	32289	0.11	0.337±0.001
DMSO	377	365	417	38176	0.58	0.495±0.004
EtOH	343	342	402	9072	0.32	0
PC	375	359	412; 430	16637	0.49	0.409±0.005

Wavelength at 340 nm was selected and the full spectrums of chromatograms were also recorded by the DAD. Starting material *trans*-4-(*N,N'*-dimethylamino)-4'-aminostilbene (DAAS) was also injected for control. Mobile phase A was 25 mM ammonium acetate while mobile phase B was acetonitrile. Gradient elution: 50 % B for the first 5 min, gradient to 85 % B in 10 min and stay for 3 min, and finally gradient back to 50 % B in 3 min and stay at 50 % B for 4 min.

## Results and Discussion

### Theoretical Calculations

Theoretical calculations were conducted with the following software suites: Gaussian 03 [12], Gaussian 09 [13] and Turbomole 6.1 [14]. The ground state studies were carried out by the density functional theory (DFT) using the Becke's Three Parameter Hybrid Method and the correlation functional of Lee, Yang, and Parr (LYP) with the correlation potentials VWM(III) (calculated in Gaussian 03 or Gaussian 09) and VWM(V) (calculated in Turbomole 6.1). The optimized

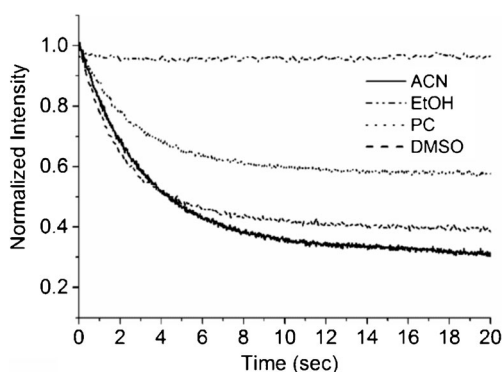


**Fig. 6** Constant-illumination fluorescence decay of DASMA to the photostationary equilibrium between *trans*- and *cis*-isomers in four solvents: AcCN, DMSO, EtOH and PC

structures were controlled by frequency calculations with the vibration analysis using a Hessian matrix. The excited states were calculated by the Time Dependent B3LYP hybrid method for the ground state optimized structures. Figure 4 shows the optimized structures of three forms of DASMA (neutral, anion and cation). The calculated properties of these structures are given in Table 2. The frequency calculations showed that all optimised isomeric structures are equilibrium ones. The vibration frequencies are positive and the number of negative Hessian is zero.

The theoretical calculations strongly support the conclusion that there is little, if any, electronic interaction between the aromatic part and the maleamic acid part of DASMA in all forms of the molecule. According to the calculations, the bond alternation is similar in all three forms, and the corresponding bond lengths of the three calculated structures are also similar. Bond distance between the nitrogen atom of the amide group and the phenyl ring is 1.4075 Å (neutral form), 1.3911 Å (anion) and 1.3991 Å (cation). The bond lengths in the amide linkage between the nitrogen and carbon atoms are 1.3814 Å (neutral form), 1.3902 Å (anion), and 1.3893 Å (cation). Thus, the amide linkage splits the molecule into two electronically decoupled fragments: stilbene with the DMA substituent, and maleamic acid. That means a chemical modification of the

maleamic acid should not affect the aforementioned fluorescence and photochrome properties of dimethylamino-stilbene. In other words, the probe should be pH-sensitive only in the relatively low to neutral (physiological) range of pH, and the maleamic acid fragment can be used to attach the probe to different systems to be tested without affecting the pH- and medium-dependent behaviour of the molecule. These speculations based on the theoretical calculations are fully supported by the experimental observations as discussed below.

Further, it can be noticed that in the anionic form, the distance between the proton of the amide linkage and one of the oxygens of the carboxylate ion is relative short (1.9277 Å) in comparison to the neutral (2.1459 Å) and cationic (2.1279 Å) forms. Such shortening of the N-H bond in this case can be explained only by formation of the intramolecular hydrogen bond. Also, this proton is strongly deshielded in the  $^1\text{H}$  NMR spectrum, supporting the formation of the intramolecular hydrogen bond, resulting in the relatively low absolute energy of the structure.

All three forms of DASMA have slightly twisted stilbene phenyl rings relative to their plane of symmetry, leading to a non-planar geometry of the molecule. Torsion angles of the phenyl rings around the stilbene double bond are 18.3° and 20.7° (neutral form), 19.4° and 10.1° (anion), and 13.6° and 8.8° (cation). As demonstrated below, such pre-twisting of the molecule in the ground state results in its relatively low fluorescence quantum yield in different solvents and fast *trans-cis* isomerisation.

In addition, a weakly hybridised dimethylamino group is observed only in the neutral and anionic forms, while in the cationic form of DASMA, it is twisted for approximately 90° relative to the plane of the phenyl ring and attains the orthogonal geometry responsible for the formation of the intramolecular charge transfer interactions in the stilbene fragment of the molecule. According to the TD-B3LYP calculations for the optimised equilibrium structure, the long wavelength transitions  $S_0 \rightarrow S_1$  have a clear charge transfer nature in DASMA cation, whilst the second fluorescence band is observed in the fluorescence emission spectrum of the cationic form.

**Fig. 7** Non-normalised (a) and normalised (b) absorption spectrum of 10  $\mu\text{M}$  DASMA in eight buffer phosphate solutions (pH 2.5–6.0)

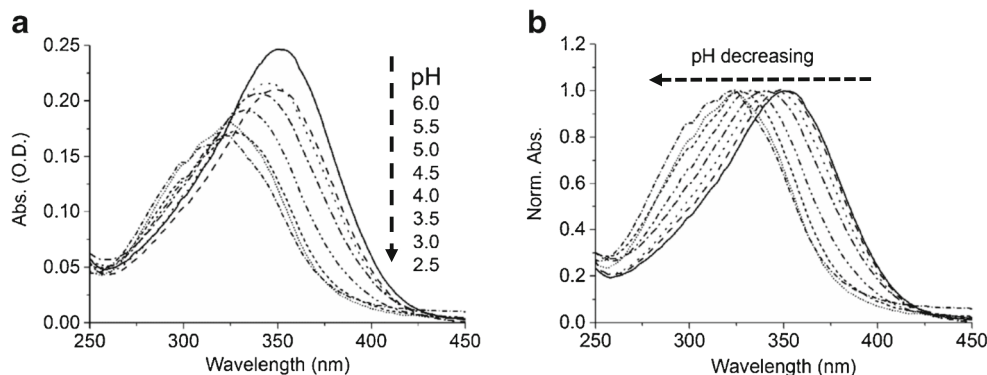
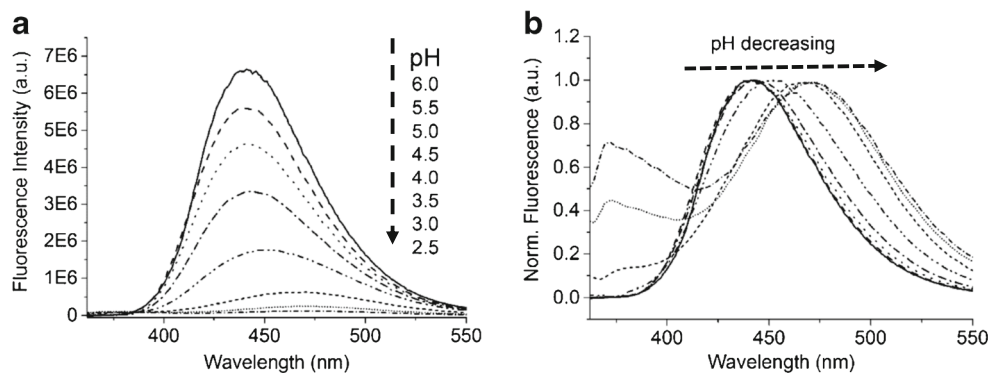


**Fig. 8** Non-normalised (a) and normalised (b) emission spectrum of 6  $\mu\text{M}$  DASMA in eight buffer phosphate solutions (pH 2.5–6.0)



Eventually, if we compare the aforementioned torsion angles of the phenyl rings around the double bond of the stilbene fragment, we can notice that the cationic form of DASMA has the most planar stilbene fragment, which is another evidence for the partial charge delocalisation and formation of the ICT in DASMA cation.

### $^1\text{H}$ NMR Studies

Chemical purity and structural identity of DASMA and its salts (anion and cation) were proved with  $^1\text{H}$  and  $^{13}\text{C}$  NMR spectra, HPLC and MALDI TOF. Chemical shifts and coupling constants were found to be in a very good agreement with the corresponding published values for the similar structures, for examples, *N*-arylmaleamic acids [10] and *N*-benzoyl aminostilbene [11], in particular, N-H at  $\delta=10.33$  ppm in DMSO  $d_6$ .

Figure 2 shows the  $^1\text{H}$  NMR spectrum of DASMA in DMSO  $d_6$  with the extension in the aromatic region between 6.2 and 7.6 ppm. Figure 3 shows the comparative  $^1\text{H}$  NMR spectra of DASMA and its salts, and Table 1 summarises the chemical shifts for three forms of DASMA. For the sake of brevity, the detailed comparison of  $^1\text{H}$  and  $^{13}\text{C}$  NMR spectra is moved to [Supplementary Information](#).

In brief, the amide proton in the anionic form is strongly deshielded and shifted to 15.3 ppm indicating the intramolecular hydrogen bonding in DASMA anion, as noted above. In addition, protons H1' and H2' of the maleamic double bond are shifted to 5.7–6.1 ppm, because they are relatively shielded by the neighbouring negative charge of the anion.

On the other hand, protons H5 and H6 of the stilbene double bond along with the phenyl ring proton H8 are deshielded by the positive charge of the DMA group in DASMA cation, and shifted to 7.2–7.3 and 7.5 ppm compared to chemical shifts of 6.9–7.0 and 6.7 ppm for the same protons of the neutral and anionic forms, respectively. Combined with twisting the DMA group and planarisation of the stilbene fragment, we assume the formation of the ICT interactions in the cationic form.

### UV Absorption and Fluorescence Spectroscopy

The absorption, excitation and emission spectra of DASMA in four different solvents are shown in Fig. 5, and Table 3 brings together all the spectroscopic properties of the molecule in these solvents at room temperature including absorption, fluorescence excitation and emission maxima, molar extinction coefficients, fluorescence quantum yields and apparent fluorescence decay rate constants ( $k_{\text{app}}$ ). Figure 6 shows the fluorescence decay kinetics of DASMA in different solvents. Mirror symmetry between excitation and emission was observed in all solvents, except propylene carbonate. Both absorption and fluorescence emission spectra of DASMA display the hypsochromic shift increased with the increase of solvent polarity, which results in a pronounced solvatochromism of the molecule. This phenomenon is usually not observed in stilbene molecules without strong donor-acceptor substituents [1, 2].

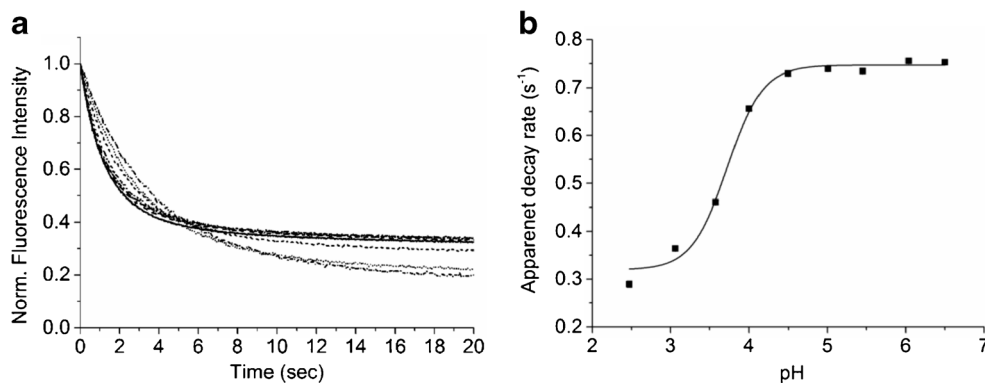
Moreover, the absorption spectrum of DASMA in all solvents, except ethanol, is blue-shifted relative to the excitation spectrum, which can be an indication of a non-emissive ICT observed at the longer wavelength in the absorption spectra of

**Table 4** Absorption and fluorescence emission maximum wavelengths, and apparent *trans-cis* photoisomerisation (fluorescence decay) rate constant for DASMA in buffer phosphate solutions having different pH values

pH	$\lambda$ (abs), nm	$\lambda$ (em), nm	$k_{\text{app}}$ , $\text{s}^{-1}$
6.5	353	441	$0.751 \pm 0.004$
6.0	350	441	$0.755 \pm 0.004$
5.5	348	441	$0.734 \pm 0.004$
5.0	343	442	$0.739 \pm 0.004$
4.5	340	444	$0.729 \pm 0.005$
4.0	332	451	$0.656 \pm 0.004$
3.5	326	465	$0.460 \pm 0.004$
3.0	323	471	$0.364 \pm 0.005$
2.5	323	472	$0.289 \pm 0.007$



**Fig. 9** pH-dependent constant-illumination fluorescence decay of 6  $\mu\text{M}$  DASMA to the photostationary equilibrium between *trans*- and *cis*-isomers in nine buffer phosphate solutions (pH 2.5–6.5) (a); and the plot of the corresponding apparent fluorescence decay rate constant vs pH (b)



the molecule. This is another unusual feature of the DASMA molecule, which we previously observed in the spectra of push-pull stilbenes [1, 2], but did not expect to observe in the present molecule.

As expected, the fast photostationary fluorescence decay of DASMA is observed in all measured polar solvents, except ethanol, and originates from the non-radiative  $^1\text{t}^* \rightarrow ^1\text{p}^*$  twisted transition, which is responsible for *trans-cis* isomerisation of the molecule and acts as a quenching funnel on fluorescence emission [1, 2].

The transition state allowed for the *trans-cis* isomerisation in the excited singlet state is expected to be polarisable and involve zwitterionic structures that lower the barrier for the twisting motion and thereby, facilitate the isomerisation reaction. In case of polar solvents, the charge separation after excitation associated with this reaction is stabilised externally by polar solvent-solute relaxation. Thus, solvent polarity affects the excited energy level of the twisted  $^1\text{p}^*$  state by stabilising its separated charges and hence, lowering the intrinsic barrier to  $^1\text{t}^* \rightarrow ^1\text{p}^*$  transition.

Therefore, for stilbenes without strong donor-acceptor substituents, the apparent isomerisation rate constant normally increases with solvent polarity, and this is because energy of more polar “phantom” state  $^1\text{p}^*$  is lowered in comparison to the energy of the *trans*-singlet state  $^1\text{t}^*$ , so the activation free energy for the *trans-cis* photoisomerisation is reduced and the apparent rate constant increases [1, 2].

Since the *trans-cis* photoisomerisation of the stilbene molecule acts as a quenching funnel on its fluorescence emission, the measured fluorescence quantum yields of DASMA in all solvents are relatively low. In other words, AcCN, DMSO and PC stabilise preferentially the  $^1\text{p}^*$  state of the molecule, thereby making the  $^1\text{t}^* \rightarrow ^1\text{p}^*$  transition faster, which in turn suppresses the radiative transition.

Regarding the spectral properties of DASMA in ethanol, absorption and emission spectra are further blue-shifted, there is no difference between excitation and absorption, and there is no observed *trans-cis* photoisomerisation. This phenomenon of strong interactions between small protic solvent

molecules and the excited state of DASMA will not be discussed in the context of the present manuscript.

### pH-Dependent Absorption and Fluorescence

Eight freshly prepared buffer phosphate solutions with pH ranging from 2.5 to 6.5 were used to investigate the effect of pH on absorption and fluorescence of the DASMA molecule. Absorption spectra shown in Fig. 7 indicate that the absorption maximum shifts to the red with increase of buffer pH, while the molar extinction coefficient  $\epsilon$  decreases.

Further, pH-dependent fluorescence emission spectra are shown in Fig. 8. There are two major trends clearly observed in the emission spectrum of DASMA when pH is lowered: fluorescence intensity significantly drops, and the maximum shifts to the blue while a new fluorescence band is developed to the red. In addition, as can be seen in Table 4, when the pH is lowered, the Stokes shift (which is the energy difference between the Franck-Condon and  $^1\text{t}^*$  states) significantly increases.

As predicted by the aforementioned theoretical calculations, the positively charged dimethylamino group twists to the orthogonal configuration and the molecule is planarised, thereby stabilising the Franck-Condon state and increasing the activation barrier for the  $^1\text{t}^* \rightarrow ^1\text{p}^*$  transition. This is reflected

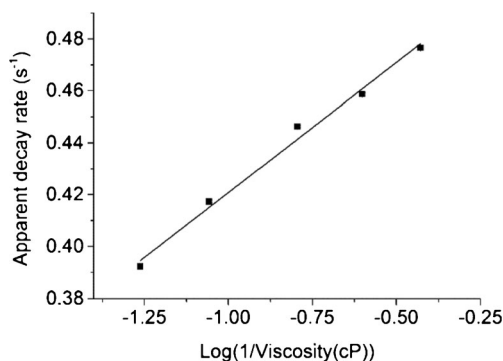


**Fig. 10** Logarithmic dependence of the apparent *trans-cis* photoisomerisation (fluorescence decay) rate constant  $k_{\text{app}}$  of DASMA on the reciprocal absolute viscosity  $1/\eta$  of the DMSO-glycerol mixtures

in the considerable decrease of the fluorescence decay rate, as can be seen in Fig. 9 showing the pH-dependent *trans-cis* photoisomerisation of the molecule (see also Table 4 for the apparent rate constants).

Nevertheless, we doubt that the formation of the second fluorescence band shifted to the red in the emission spectrum of DASMA at low pH can be attributed to the twisted intramolecular charge transfer in the excited state [15–18]. However, we cannot exclude this possibility, as well as any other possibility including solvation effects, hydrogen bonding or even formation of dimers.

### Medium Viscosity Study

As noted above, the apparent *trans-cis* photoisomerisation rate constant is strongly dependent on medium properties, such as microviscosity [5]. Figure 10 shows the logarithmic dependence of the fluorescence decay rate (apparent *trans-cis* photoisomerisation rate constant) of DASMA on the reciprocal absolute viscosity  $1/\eta$  in a series of DMSO and glycerol mixtures. Such dependence of the  $k_{app}$  value on viscosity of the medium suggests that DASMA, as other stilbene molecules, can be a useful indicator for local microviscosity in various condensed media. The logarithmic

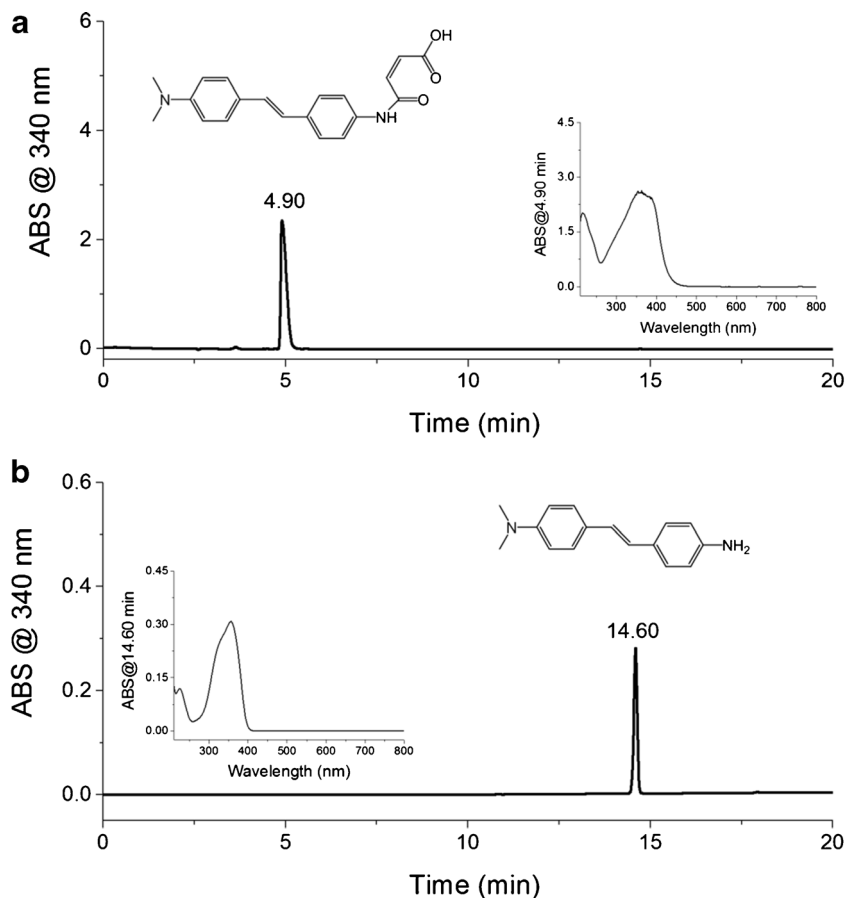
dependence of  $k_{app}$  on  $1/\eta$  of a solvent may be used as a calibration curve for the microviscosity determination in the vicinity of the probe. This technique is very sensitive compared to other well-known techniques for determination of microviscosity, like fluorescence, spin- or triplet-photochrome methods [20]. It allows to measure the microviscosity in the vicinity of DASMA at sub-nanomolar concentrations.

### RP-HPLC Chromatograms and UV Spectra

The HPLC chromatograms and corresponding UV spectra at peak position of DASMA and DAAS are shown in Fig. 11. Compared to DAAS having a retention time (RT) of 14.60 min, DASMA has a RT of 4.90 min. This decrease in RT of DASMA indicates an increase in polarity due to the introduction of the maleamic acid group. According to the aforementioned theoretical calculations, the molecule has a dipole moment of 1.50 D (see Table 2).

Additionally, the chromatogram of DASMA indicates a high purity (>99 %) of the synthesised product and confirms its chemical identity, while only traces of the starting material DAAS were detected.

**Fig. 11** RP-HPLC chromatograms and UV spectra of **a** DASMA and **b** DAAS



## Conclusions

In the present study, DASMA and its ammonium and hydrochloride salts were successfully synthesised, purified and characterised by  $^1\text{H}$  and  $^{13}\text{C}$  NMR, and mass spectroscopy.

Theoretical studies of DASMA, its anion and cation, showed that the amide linkage splits the molecule into two electronically decoupled fragments: stilbene with the DMA substituent, and maleamic acid. That means a chemical modification of the maleamic acid should not affect the fluorescence and photochrome properties of dimethylamino-stilbene, and the probe is pH-sensitive only in the low to neutral range. Thus, the maleamic acid fragment can be used to attach the probe to different systems to be tested without affecting the pH- and medium-dependent behaviour of the molecule.

Spectroscopic studies of DASMA evidenced the fast photostationary fluorescence decay of the molecule observed in all measured polar solvents, except ethanol, and originating from the non-radiative  $^1\text{t}^* \rightarrow ^1\text{p}^*$  twisted transition, which is responsible for *trans-cis* isomerisation of the molecule and acts as a quenching funnel on fluorescence emission.

We found that DASMA exhibits the pH-dependent fluorescence in a physiological range of pH. Even more important, the apparent fluorescence decay rate constant also shows this dependence, making DASMA probably the first pH-sensitive photochrome probe.

In addition, we proved that DASMA can be used as a sensitive indicator for local microviscosity in various condensed media. Thus, we can conclude that we developed a unique molecular photochrome probe that exhibits solubility and retains conformational flexibility in a wide range of organic solvents and aqueous pH environments. With a ‘click chemistry’ the functional group of the molecule can be incorporated for ease of chemical grafting, while the molecular sensing group can monitor changes in both pH- and microviscosity simultaneously.

**Acknowledgments** This research is funded by the Singapore National Research Foundation and the publication is supported under the Campus for Research Excellence and Technological Enterprise (CREATE) programme (13-04-00364 A). Funding was also greatly appreciated from the Ministry of Education Tier 1 Grant: *Photochrome aptamer switch assay: A universal bioassay device* - RG54/13.

## References

- Papper V, Pines D, Likhstenshtein GI, Pines E (1997) Photophysical characterisation of *trans*-4,4'-disubstituted stilbenes. *J Photochem Photobiol A Chem* 111:87–96
- Papper V, Likhstenshtein G (2001) Substituted stilbenes: a new view on well-known systems: new application in chemistry and biophysics. *J Photochem Photobiol A Chem* 140:39–52
- Ahluwalia A, De Rossi D, Giusto G, Chen O, Papper V, Likhstenshtein GI (2002) A fluorescent-photochrome method for the quantitative characterization of solid phase antibody orientation. *Anal Biochem* 305:121–134
- Likhstenshtein GI, Bishara R, Papper V, Uzan B, Fishov I, Gill D, Parola AH (1996) Novel fluorescence-photochrome labelling method in study of biomembrane dynamics. *J Biochem Biophys Methods* 33:117–133
- Strashnikova N, Papper V, Parkhomyuk-Ben Arye P, Likhstenshtein GI, Ratner V, Marks R (1999) Local medium effects in the photochemical behaviour of substituted stilbenes immobilized on quartz surface. *J Photochem Photobiol A Chem* 122:133–142
- Horiba Scientific, NIST develops fluorescence standards with FluoroLog<sup>®</sup>, Fluorescence Technical Note FL-30. [http://www.horiba.com/fileadmin/uploads/Scientific/Documents/Fluorescence/FL-30\\_NIST\\_Fluorolog.pdf](http://www.horiba.com/fileadmin/uploads/Scientific/Documents/Fluorescence/FL-30_NIST_Fluorolog.pdf). Accessed 27 July 2014
- Meech SR, Phillips D (1983) Fluorescence standards. *J Photochem* 23:193–207
- Papper V, Wu Y, Kharlanov V, Sukharaharja A, Steele TWJ, Marks RS (2014) Theoretical and experimental studies of N,N-dimethyl-N'-picryl-4,4'-stilbenediamine. *J Fluoresc*. doi:10.1007/s10895-014-1425-9
- Papper V, Pokhonenko O, Wu Y, Zhou Y, Jianfeng P, Steele TWJ, Marks RS (2014) Novel photochrome aptamer switch assay (PHASA) for adaptive binding to aptamers. *J Fluoresc* 24(6):1581–1591
- Trujillo-Ferrara J, Correa-Basurto J, Espinosaa J, Garciaa J, Martinezb F, Mirandac R (2005) Solvent-free synthesis of arylamides and arylimides, analogues of acetylcholine. *Synth Commun* 35(15):2017–2023
- Lewis FD, Liu W (1999) Luminescence of N-arylbenzamides in low-temperature glasses. *J Phys Chem A* 103(48):9678–9686
- Frisch MJ, Trucks GW, Schlegel HB, Scuseria GE, Robb MA, Cheeseman JR, Montgomery JA Jr, Vreven T, Kudin KN, Burant JC, Millam JM, Iyengar SS, Tomasi J, Barone V, Mennucci B, Cossi M, Scalmani G, Rega N, Petersson GA, Nakatsuji H, Hada M, Ehara M, Toyota K, Fukuda R, Hasegawa J, Ishida M, Nakajima T, Honda Y, Kitao O, Nakai H, Klene M, Li X, Knox JE, Hratchian HP, Cross JB, Bakken V, Adamo C, Jaramillo J, Gomperts R, Stratmann RE, Yazyev O, Austin AJ, Cammi R, Pomelli C, Ochterski JW, Ayala PY, Morokuma K, Voth GA, Salvador P, Dannenberg JJ, Zakrzewski VG, Dapprich S, Daniels AD, Strain MC, Farkas O, Malick DK, Rabuck AD, Raghavachari K, Foresman JB, Ortiz JV, Cui Q, Baboul AG, Clifford S, Cioslowski J, Stefanov BB, Liu G, Liashenko A, Piskorz P, Komaromi I, Martin RL, Fox DJ, Keith T, Al-Laham MA, Peng CY, Nanayakkara A, Challacombe M, Gill PMW, Johnson B, Chen W, Wong MW, Gonzalez C, Pople JA (2004) Gaussian 03, revision C.02. Gaussian, Inc, Wallingford
- Frisch MJ, Trucks GW, Schlegel HB, Scuseria GE, Robb MA, Cheeseman JR, Montgomery JA Jr, Vreven T, Kudin KN, Burant JC, Millam JM, Iyengar SS, Tomasi J, Barone V, Mennucci B, Cossi M, Scalmani G, Rega N, Petersson GA, Nakatsuji H, Hada M, Ehara M, Toyota K, Fukuda R, Hasegawa J, Ishida M, Nakajima T, Honda Y, Kitao O, Nakai H, Klene M, Li X, Knox JE, Hratchian HP, Cross JB, Bakken V, Adamo C, Jaramillo J, Gomperts R, Stratmann RE, Yazyev O, Austin AJ, Cammi R, Pomelli C, Ochterski JW, Ayala PY, Morokuma K, Voth GA, Salvador P, Dannenberg JJ, Zakrzewski VG, Dapprich S, Daniels AD, Strain MC, Farkas O, Malick DK, Rabuck AD, Raghavachari K, Foresman JB, Ortiz JV, Cui Q, Baboul AG, Clifford S, Cioslowski J, Stefanov BB, Liu G, Liashenko A, Piskorz P, Komaromi I, Martin RL, Fox DJ, Keith T, Al-Laham MA, Peng CY, Nanayakkara A, Challacombe M, Gill PMW, Johnson B, Chen W, Wong MW, Gonzalez C, Pople JA (2004) Gaussian 09, revision A.02. Gaussian, Inc, Wallingford
- Ahrlrichs R, Bär M, Baron H-P, Bauernschmitt R, Böcker S, Deglmann P, Ehrig M, Eichkorn K, Elliott S, Furche F, Haase F, Häser M, Hom H, Hättig Ch, Huber Ch, Huniar U, Kattannek M, Köhn

- A, Kölmel Ch, Kollwitz M, May K, Ochsenfeld Ch, Öhm H, Schäfer A, Schneider U, Sierka M, Treutler O, Unterreiner B, von Amim M, Weigend F, Weis P, Weiss H (2008) Turbomole 5.9. Karlsruhe
15. Gilibert E, Lapouyade R, Rulliere C (1988) Dual fluorescence in 4-dimethylamino-4'-cyanostilbene revealed by picosecond time-resolved spectroscopy. *Chem Phys Lett* 145:262–267
  16. Lapouyade R, Czeschka K, Majenz W, Rettig W, Gilibert E, Rulliere C (1992) Photophysics of donor-acceptor substituted stilbenes. *J Phys Chem* 96:9643–9650
  17. Le Breton H, Bennetau B, Letard J-F, Lapouyade R, Rettig W (1996) Non-radiative twisted intramolecular charge transfer state in polar stilbenes. *J Photochem Photobiol A Chem* 95:7–20
  18. Il'ichev YV, Zachariasse KA (1997) Intramolecular charge transfer, isomerization and rotational reorientation of trans-4-dimethylamino-4'-cyanostilbene in liquid solution. *Ber Bunsenges Phys Chem* 101:625–635
  19. Steele TWJ, Shier WT (2010) Dendrimeric alkylated polyethylenimine nano-carriers with acid-cleavable outer cationic shells mediate improved transfection efficiency without increasing toxicity. *Pharm Res* 27(4):683–698
  20. Likhtenshtein GI (2009) Novel fluorescent methods for biotechnological and biomedical sensing: assessing antioxidants, reactive radicals, no dynamics, immunoassay, and biomembranes fluidity. *Appl Biochem Biotechnol* 152(1):135–155